Available online at www.sciencedirect.com
SCIENCE DIRECT
Carbohydrate Research 341 (2006) 492–498
Carbohydrate RESEARCH

Sucrose solution freezing studied by magnetic resonance imaging

Rachid Mahdjoub,[a] Pierre Chouvenc,[b,c] Marie José Seurin,[a,*] Julien Andrieu[b] and André Briguet[a]

[a]*Laboratoire de RMN, UMR5012 CNRS, Université Claude Bernard Lyon 1, ESCPE, 43 bd du 11 Novembre 1918, 69616 Villeurbanne cedex, France*
[b]*LAGEP, UMR5007 CNRS, Université Claude Bernard Lyon 1, ESCPE, 43 bd du 11 Novembre 1918, 69616 Villeurbanne cedex, France*
[c]*Aventis Pasteur, Campus Mérieux, 1541 av Marcel Mérieux, F-69280 Marcy l'Etoile, France*

Received 12 June 2005; received in revised form 4 January 2006; accepted 5 January 2006
Available online 23 January 2006

Abstract—Ice formation of a 20% w/v sucrose solution was monitored during the freezing process by magnetic resonance imaging (MRI). An original experimental setup was designed with oil as a cooling fluid that allows accurate control of the temperature. The NMR signal intensity of particular sampled volumes was observed during the entire cooling period, from 0 to −50 °C, showing a peak characteristic to a transition before the loss of the signal. Moreover, spatial ice distribution of the frozen matrix was observed by high resolution MRI with an isotropic resolution of $78 \times 78 \times 78$ μm^3. MRI has proved to be a novel technique for determining the glass transition temperature of frozen sucrose solutions, in the concentration range where calorimetric measurements are not feasible.

Keywords: Sucrose solution; Glass transition; Ice formation; Ice structure; NMR microimaging

1. Introduction

Freezing is an important means of preserving foods and other biological materials. The quality of thawed food products (like fish,[1,2] meat,[3,4] fruits[5,6]) depends on an irreversible freezing process because cell deteriorations are generated. The lyophilization process requires the characterization of the frozen matrix.[7] In other areas, the cryo-conservation of semencea of animal species[8] or of organs[9] has to be a well-controlled process. Whenever possible, ice crystallization damages have to be avoided for all of these processes by using, for example, vitrification where a glassy state forms instead of ice formation. For this, it is necessary to know exactly the state diagram of the studied solution upon cooling and particularly the T_m value (temperature for the appearance of the first ice crystal) and T_g value (the temperature at which the viscosity of the unfrozen liquid phase becomes a limiting factor for the growth of the size of ice crystals, that is, the solution turns from the liquid state to a glassy one).

Magnetic resonance imaging (MRI) allows the visualization of the freezing process following the spatial distribution of non-frozen water for samples placed in a cold air flow.[10] This feasibility for determining the liquidus curve by NMR was explored from 1989, on sucrose solutions by Harz et al.[11] The general relationship between the NMR signal intensity and the structure of a solution is given by

$$U(t) = U_{0,s}\exp(-(t/2(T_{2,s}))^2)U_{0,l}(\exp(-t/T_{2,l})) \quad (1)$$

where $U_{0,s}$ and $U_{0,l}$ are the maximal intensity of the signal of the solution in the solid and in the liquid, respectively, and $T_{2,s}$ and $T_{2,l}$ the spin–spin relaxation time, respectively, for the two forms. Different components may be encountered if protons belong to different molecules (sugar protons and water protons) and/or if they

* Corresponding author. E-mail: seurin@univ-lyon1.fr

0008-6215/$ - see front matter © 2006 Elsevier Ltd. All rights reserved.
doi:10.1016/j.carres.2006.01.005

are involved in different physical states (liquid or solid). Thus, the NMR signal intensity of an aqueous mixture reflects the amount of water in both the liquid (unfrozen water) and solid states (ice) during cooling.[12]

In imaging experiments with a classical spin-echo sequence, the relaxation signal intensity S is given by

$$S \propto \rho(1 - e^{-TR/T_1})e^{-TE/T_2} \quad (2)$$

with TR (repetition time) and TE (echo time) are imaging parameters, T_1 spin–lattice relaxation time and T_2 spin–spin relaxation time specifics of the studied proton. It is known that temperature influence reflects principally on T_1 assessment, the effect used in thermometry. So, upon cooling, the liquid relaxation signal intensity decreases because of many factors such as temperature decreases and its direct effect on relaxation time values, the decrease in the liquid water amount and also the cryo-concentration of the remaining liquid. However, monitoring the freezing kinetics of a sucrose solution is possible, by studying the cooling curve, which depicts 'global signal' intensity evolution as a function of cooling time, that is, as function of temperature.

Previous literature has indicated that the ice phase in sucrose solutions is pure water only and that the conformation of aqueous sucrose does not depend on temperature and or initial sucrose concentration.[13] Usually, the experimental glass transition temperature values (T_g) are obtained from differential scanning calorimetry (DSC) for sucrose solutions, but only for highly concentrated sucrose solutions (over 65/35 sucrose/water).[14] The slower the cooling process, the more time the crystals have to grow and the T_g value of the solution decreases. The cooling rate is a determinant factor for the molecular rearrangement and for fast freezing the T_g values are easily measurable. For example, a cooling rate equal to 20,000 °C/s is necessary to vitrify pure water.[15] Some literature data for sucrose solutions and pure compounds[16] are reported in Table 1 and were used to produce the sucrose/water phase diagram in Figure 1. Roos[14] has used Gordon and Taylor's formulae, which allows calculation of T_g values for binary polymer mixtures, to obtain the theoretical curve of T_g values of carbohydrates at various water contents, reported in Figure 1.

The present state-of-the-art does not make it possible to choose between T_g equal to −33 °C predicted from the extrapolation of the experimental results or T_g equal

Table 1. T_m and T_g values for some different concentrations of sucrose/water solutions (% in w/v); the experimental values have been obtained with a cooling rate of 10 °C/min

Compound	T_m (°C)	T_g (°C)	Method	Literature data
Pure sucrose	192	66	Experimental DSC	Blond et al.[16]
80% Sucrose		−46	Experimental DSC	Roos[14]
70% Sucrose		−68	Experimental DSC	Roos[14]
55% Sucrose	−5.5	Around −35	Experimental DSC	Blond et al.[16]
20% Sucrose	−1.5	−125	Theoretical	Blond et al.[16]
Pure water	0	−135		Johari et al.[15]

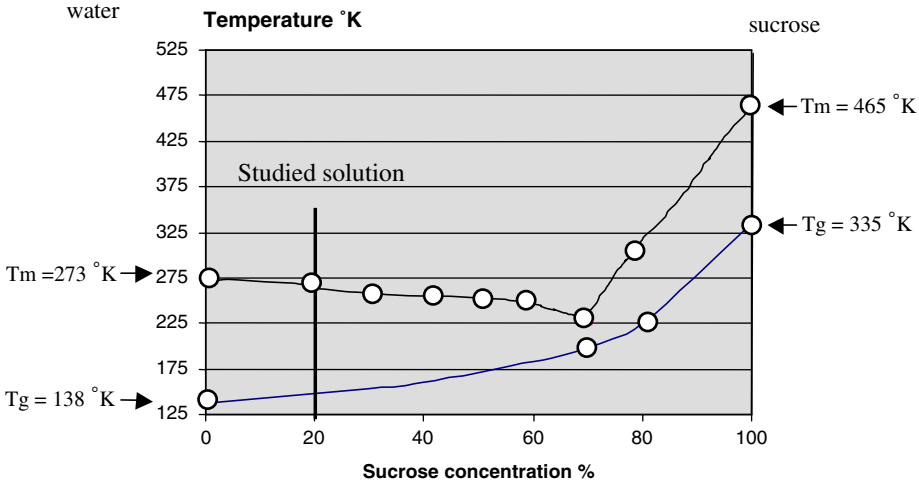

Figure 1. Concentration–temperature state diagram for aqueous sucrose solutions (data[16]): (○) experimental data, (—) theoretical lines (calculated with the Gordon and Taylor's formulae $T_g = \frac{\omega_1 T_{g1} + k\omega_2 T_{g2}}{\omega_1 + k\omega_2}$ where ω_1 and ω_2 are the weight fractions of the solute and water, respectively, T_{g1} is the T_g of the anhydrous solute, T_{g2} is the T_g of water and k is a constant (for sucrose $k = 5.12$)). All temperatures are in kelvin.

to −125 °C obtained from theoretical model, for a 20% sucrose solution. The aim of this MRI study is to try to resolve this question by monitoring, in situ and non-invasively, the freezing of this solution. Quantitative analysis of the signal acquired during freezing of a 20% w/v sucrose solution was performed and highly spatially resolved images of the frozen matrix were obtained.

2. Materials and methods

2.1. Samples

The model used was an aqueous solution with 20% w/v of sucrose (Sigma Aldrich, USA, $M_W = 342.49$) in a 7 mL glass vial, with the outer and inner diameters being 20 and 18 mm, respectively. The vial was filled with 2.5 mL of the solution, corresponding to a 10 mm height.

For dynamic studies, (i.e., in situ monitoring of NMR signal intensity with decreasing temperature) samples were pre-cooled to 0 °C and then frozen to −50 °C. High-resolution MRI studies were performed on samples uni-directionally frozen to −50 °C. The sample was then immersed into liquid nitrogen to stabilize the structure of the frozen matrix. During imaging experiments, the sample temperature was fixed at −20 °C.

2.2. Cooling system

The cooling system, which was specifically developed for this experiment, consisted of a cooling apparatus (cryostat Bioblock, Huber CC180, Germany) with a −80 to 100 °C range, and a beaker-like vessel containing both the coil and the sample. Cooling fluid (silicone oil) was circulated in the double jacket of the beaker. This cooling system and the beaker were linked with two silicone pipes of 10 mm inner diameter. The evolution of freezing power as a function of the temperature is provided by the manufacturer. The temperature as a function of cooling time is given by

$$\theta = 6.10^{-7}(t^2) - 0.0202(t) \quad (3)$$

where θ is the temperature in °C and t the cooling time in seconds.

2.3. MRI

The MRI experiments were performed on an Oxford 2 T magnet with 50 mT/min gradients. For dynamic studies, the bottom of the vial was placed on a freezing surface, and thus the reference temperature was fixed in a one-dimensional freezing model. The vial and the coil both had to be approximately at the same level above this surface. Therefore, a six turn transmitter–receiver solenoidal coil of 15 mm length and 20 mm diameter was built specifically according to the sample size and tuned to 85.13 MHz (^{1}H frequency) as shown in Figure 2a. To limit resistive losses, the windings were spaced out to reduce the proximity effect and a 2 mm diameter wire was used to minimize the skin effect losses.[17] To cancel signals from hydrogen nuclei in the silicone oil used as cooling fluid, a Faraday shield was inserted between the cooling fluid chamber and the solenoid (Fig. 2b). Matching the resonator to the preamplifier was done using an inductive loop.

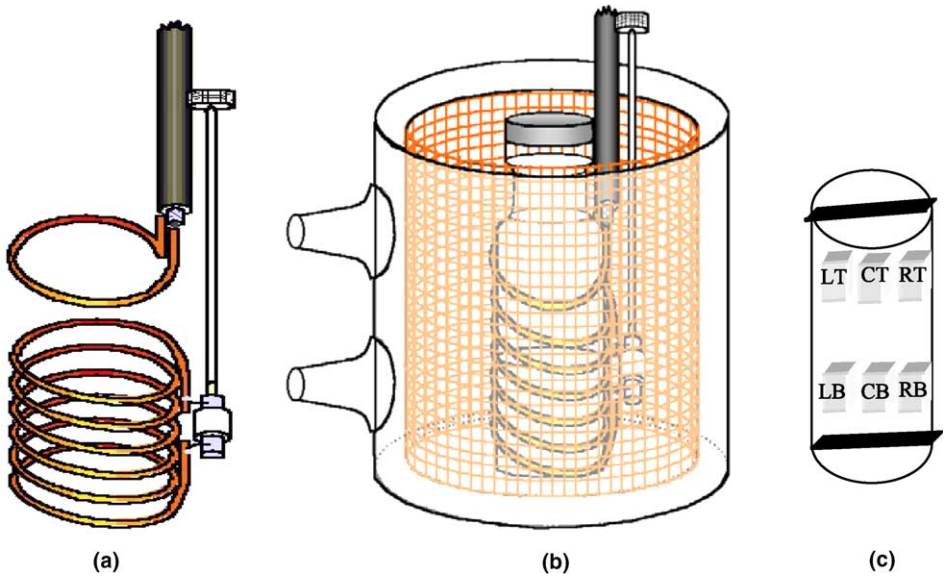

Figure 2. Solenoidal radiofrequency coil used for NMR measurements: (a) length = 15 mm, diameter = 20 mm, wire diameter = 2 mm, number of turns = 6; (b) Location of the NMR coil inside the double jacket beaker; (c) volumes of interet (VOI) studied during kinetics. L = left; C = centre; R = right; B = bottom; T = top.

A conventional spin-echo sequence was used for continuous acquisition of a set of images during the cooling process. The relaxation times of different protons can be estimated from the literature data, that is, at 4 °C, for sugar protons $T_2 \sim 58$ ms and $T_1 \sim 94$ ms, and for water protons $T_2 \sim 485$ ms and $T_1 \sim 636$ ms.[18] This knowledge makes it possible to choose relevant values of the imaging parameters TE and TR to reduce the acquisition time per image. Two series of kinetic studies were made for each sample, hereafter referred to as kinetics A and kinetics B. For kinetics A (Fig. 3a), parameters values were: TE = 16 ms, TR = 100 ms, data matrix = 128×32, field of view = 19×19 mm, slice thickness = 1 mm and 2 averages. The acquisition time was 6.4 s per image and 425 images were acquired during the first 45 min 20 s of the freezing process (from 0 to −50 °C). To increase temporal resolution, kinetics B, shown in Figure 3b, used the parameter values: TE = 15 ms, TR = 50 ms, data matrix = 128×32, field of view = 19.3×19.3 mm, slice thickness = 2 mm and only one acquisition. The acquisition time was 1.6 s per image and 825 images were acquired during 22 min, starting 10 min after the beginning of the freezing process (from −12 to −50 °C).

To obtain a high signal to noise ratio, the parameter values of the three dimensional spin-echo sequence were chosen as following: TE = 16 ms, TR = 120 ms, data matrix = $256 \times 256 \times 256$, field of view = $20 \times 20 \times 20$ mm and 8 averages. The spatial resolution (voxel size) was $78 \times 78 \times 78$ (μm)^3.

2.4. Image processing

Magnitude images were reconstructed by direct Fourier Transform of the raw data. For each dynamic study, proton signal evolution as a function of time was performed at six different locations in the sample as shown in Figure 2c.

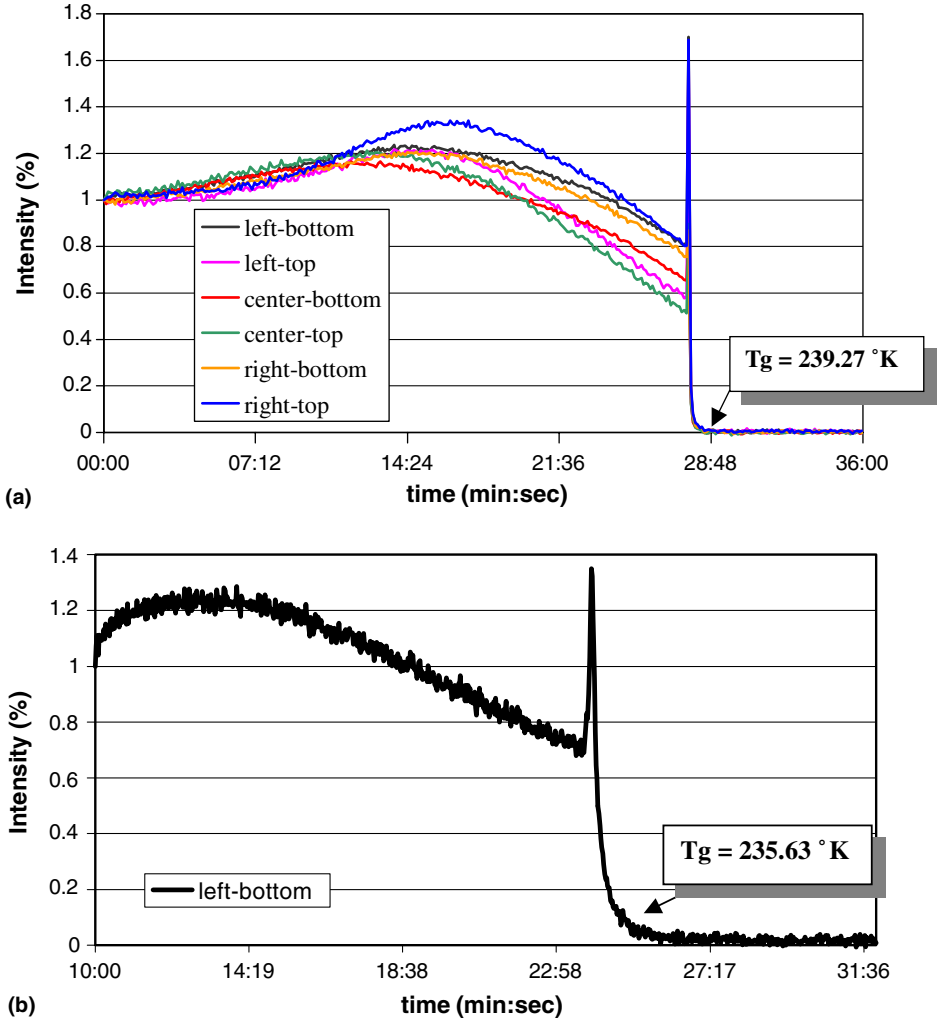

Figure 3. (a) Kinetics A for the six VOI of the solution (cf. Fig. 2c) with a resolution of 6.4 s/point. The time is related to the cooling temperature by Eq. (1). (b) Kinetics B for one VOI of the solution (e.g., LB) with a resolution of 1.6 s/point.

3. Results and discussion

3.1. Kinetics of the cooling of a sucrose solution

Signal intensity variations were nearly identical in the six selected volumes of interest VOI (Fig. 3a). During kinetics A and B, the signal intensity first increased before decreasing slowly and was broken up by a spiked peak. The hump observed after 14 min (Fig. 3a and b) can be explained by Curie's law, which predicts that the magnetization varies as a function of $1/T$ (S increasing) but also as a progressive loss of molecular mobility in a medium that is becoming more and more motionless while the temperature of the sample decreases (S decreasing). This apparent continuous sample evolution may also be caused by convective flow due to the temperature gradients inside the sample. The spiked peak was followed by an abrupt signal drop. This last effect is believed to be caused by a phase transition of the solution from a glass to the solid state. For kinetics A, this very fast phenomenon happened after 28 min of cooling period, that is, at 239.3 K, with a duration less than 13 s.

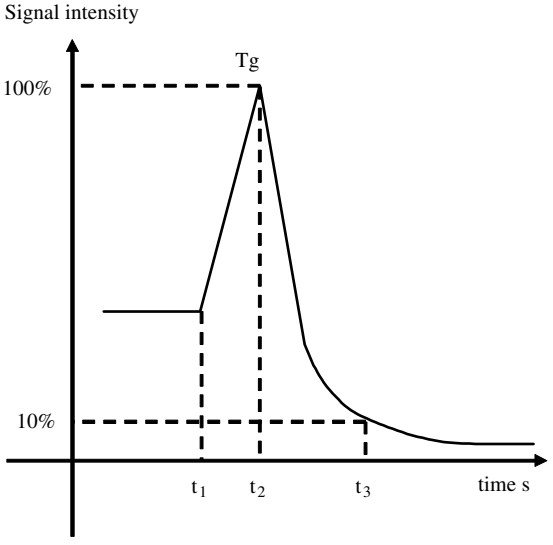

Figure 4. Schematic description of the observed peak and definition of times referenced in text: t_1 = beginning of the transition, the viscosity value of the solution is maximum, $t_2 = T_g$ glass transition temperature, t_3 = end of the sample crystallization.

The spiked peak was also observed using an acquisition time per image of 1.6 s, that is, kinetics B (Fig. 4b). The intense peak emergence could be observed 14 min after the beginning of the data acquisition (data collection started 10 min after the beginning of the sample cooling), that is, at 235.6 K. The discrepancy between 28 and 24 min, and the non-equal temperatures −33.7 and −37 °C, respectively, may be due to differences in the freezing ramp period. In the first case (28 min, −33.7 °C), the freezing ramp was chosen from 0 to −50 °C with a 6.4 s acquisition interval while a freezing ramp from −12 to −50 °C with a 1.6 s acquisition interval was taken in the second one (24 min, −37 °C). This transient state was represented as a sharp intensity peak followed by a rapid exponential-like drop towards zero with a time constant τ in the order of 11 s (Fig. 4). Starting from the beginning of the cooling experiment, three characteristic times have been defined: t_1 corresponds to the origin of the peak, t_2 to the top of the peak and t_3 the time of the decay. Notice that t_2 corresponds to the glassy-solid transition temperature designed as T_g. An original observation was that the beginning of the transition started at the same time (values of t_1 and t_2 in Table 2) through the whole volume of the sample.

As expected, the crystallization time, which is characterized by $t_3 - t_2$, was found to be shorter at the bottom sample than at the top and shorter at the centre of the sample than at sides (Table 2 and Fig. 5). We note that the beaker was open to the atmosphere and cold losses could occur at its surface top. These observations are in accordance with the presence of the cooling gradient from bottom to top.

At time t_1, the viscosity of the sucrose solution is at its maximum and molecules rearrange to allow crystallization, which is an exothermic process. The temperature increases rapidly from the nucleation temperature up to the freezing equilibrium temperature.[19] Due to a supercooling effect, water molecules retrieve some mobility leading to a high intensity NMR signal. This crystallization process has been associated with a convective mass flow moving molecules present in the liquid state.[20] In this hypothesis, water molecules diffuse through the liquid matrix towards the surface of ice crystals, while sucrose molecules are excluded from the

Table 2. Characteristic times for kinetics B, as defined in text: t_1 corresponds to the beginning of the peak and t_2 to the maximum of the peak

Position	t_1 (min:s)	t_2 (min:s)	t_3 (min:s)	$\Delta t = t_2 - t_1$	$\Delta t' = t_3 - t_2$
Left-top	23:45.6	23:56.8	25:36.0	11.2	100
Left-bottom	23:45.6	23:56.8	24:38.4	11.2	42
Centre-top	23:45.6	23:56.8	25:05.6	11.2	70
Centre-bottom	23:45.6	23:56.8	24:27.2	11.2	31
Right-top	23:45.6	23:55.2	25:29.6	9.6[a]	94
Right-bottom	23:45.6	23:55.2	24:38.4	9.6[a]	43

Freezing rates, characterized by t_3 values, were higher at the bottom than at the top of the sample (precision ± 1.6 s).
[a] Due to cooling jacket beaker conception, the cooling flux was coming from the same side (here, the right side).

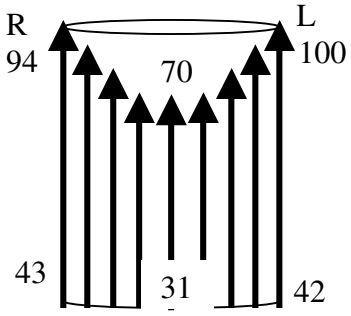

Figure 5. Temperature gradients in the vial.

surface of the ice crystals. This reorganization time is given by $\Delta t = t_2 - t_1$ (mean value of 10.67 ± 1.6 s). Finally, the intensity drop as a function of time may be used to quantify ice crystallization rate (τ value) and crystallization duration values, given by $\Delta t' = t_3 - t_2$ (Table 2).

3.2. Structure of a cooling sucrose solution

Three-dimensional images with an isotropic spatial resolution of 78 μm (Fig. 6a and b) show the internal structure of two samples of a frozen opaque 20% w/v sucrose solution. After freezing to −50 °C and storing in liquid nitrogen, the sample was kept for 5 h at −20 °C inside the magnet bore to stabilize the temperature before the NMR experiment. This temperature is above the glass transition temperature ($g = -35 \pm 2$ °C) of the solution. The sample structure can be considered as a compromise between a solid frozen ice structure, and a viscous concentrated phase containing a sucrose solution where hydrogen nuclei mobility allows the observation of a NMR signal. Unfortunately, the acquisition time for such NMR microimaging is generally more than 20 h. Under such conditions, Ostwald ripening may occur leading to ice crystal size increases by clustering. This recrystallization phenomenon is driven by a chemical potential force, which tends to minimize the surface energy.[19] This phenomenon was widely observed and studied in the frozen food area, especially in ice-cream storage.[21,22] Such an image does not give a precise view of the structure of the ice network in this particular sample. White areas are rich in motion-free hydrogen nuclei and correspond to a viscous phase. In dark areas

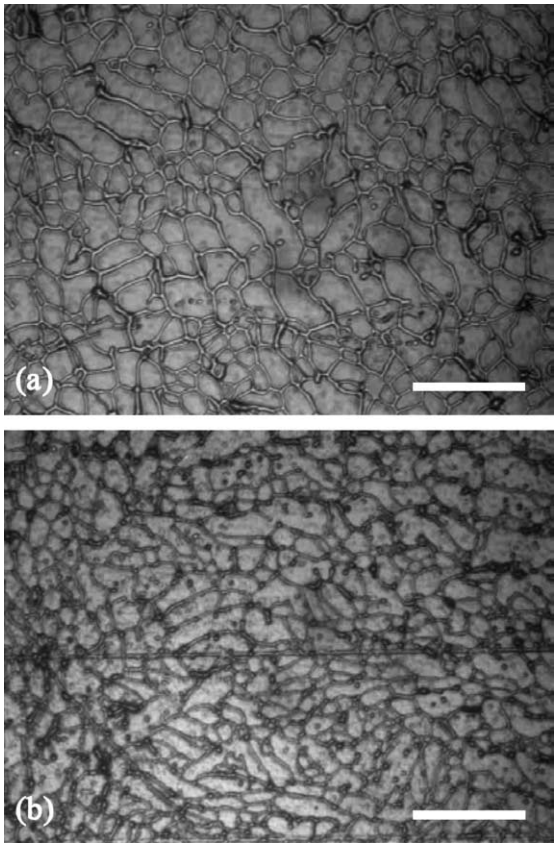

Figure 7. Observation by reflection microscopy of a 10% w/v solution of sucrose frozen in a 7 mL vial. Ice appears as gray areas and the cryo-concentrated matrix appears here as dark channels: (a) observation of the middle of the sample and (b) observation at the bottom of the sample. Scale = 265 μm.

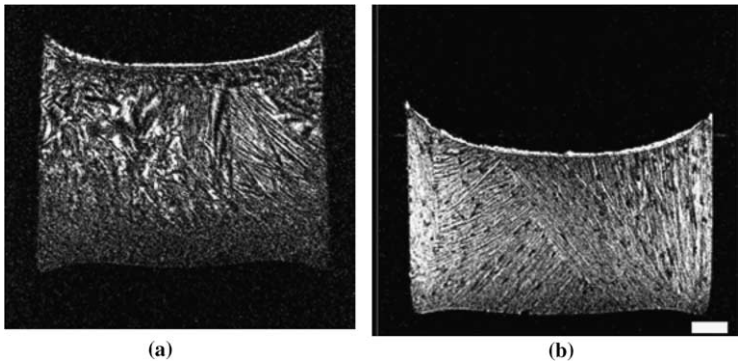

Figure 6. Internal structures of a frozen sucrose solution. A thin layer (thickness = 300 μm) of highly concentrated in sucrose, can be observed at the surface of the sample. It may be possible to observe: (a) a sheet-like ice crystal pattern on the left side, sucrose aggregates on the right side and a thinner structure at the bottom of the sample; (b) a more regular sheet-like ice crystal pattern and bigger cylindrical ice channels. Scale = 2 mm.[23]

hydrogen nuclei are bound to solid ice. Aggregates and sheet-like white zones can be observed inside the whole sample, which appears heterogeneous. Moreover, no ice structure can be observed at the bottom of the sample because the ice crystals are too small compared to the spatial resolution of images. This phenomenon can be explained by primary nucleation, which generates small ice crystals from the liquid phase, and occurred preferentially at the vial bottom where the under-cooling degree was a maximum. This ice structure pattern has also been confirmed by reflection microscopic studies of the frozen matrix[23] as shown in Figure 7. A concentrated sucrose layer of approximately 300 μm thickness, was observed at the surface of the sample. This 'crust effect' was probably due to the diffusion of sucrose from ice crystals to the thin layer during crystallization process.[24] Therefore, the high resolution MRI technique permitted the observation of the main patterns of the freezing process.

4. Conclusion

Freezing used in food storage, cryopreservation of living systems and other areas must be an irreversible phenomenon because ice crystallization leads to cell deteriorations. MRI is able to image the freezing process after the solution becomes opaque due to ice formation. In addition the technique can probe the final microstructure of the solution non-invasively. For this, an original setup of a temperature ramp probe has been described here to allow freezing phenomena to be studied in situ in the magnet. This experiment has been performed on a binary system (20 sucrose/80 water). The kinetic studies with short acquisition times (1.6 s/image) showed the evolution of sucrose and water molecules in solution before the glass phase transition leading to the crystallization of the whole sample. The glass transition temperature T_g and the duration of crystallization phenomena have been evaluated. These preliminary results prove that MRI may be employed for the determination of state diagram of sucrose solutions, in a range of concentrations, which is not available by other techniques. Moreover MRI microscopy with an isotropic resolution of $78 \times 78 \times 78$ μm^3 is also able to characterize dendritic ice structure and reveals some patterns of ice channels and sucrose in the sample. These observations are in accordance with two-dimensional information on the matrix structure obtained using reflection microscopy.

References

1. Howell, N.; Shavila, Y. *J. Sci. Food Agric.* **1996**, *72*, 49–56.
2. Nott, K. P.; Evans, S. D.; Hall, L. D. *Magn. Reson. Imaging* **1999**, *17*, 445–455.
3. Evans, S. D.; Nott, K. P.; Kshirsagar, A. A.; Hall, L. D. *Int. J. Food Sci. Technol.* **1998**, *33*, 317–328.
4. Renou, J. P.; Foucat, L.; Bonny, J. M. *Food Chem.* **2003**, *82*, 35–39.
5. Evans, S. D.; Brambilla, A.; Lane, D. M.; Torreggiani, D.; Hall, L. D. *Lebensm. Wiss. Technol.* **2002**, *35*, 177–184.
6. Kerr, W. L.; Clark, C. J.; McCarthy, M. J.; De Ropp, J. S. *Sci. Hortic.* **1997**, *69*, 169–179.
7. Hottot, A.; Vessot, S.; Andrieu, J. *PDA J. Pharm. Sci. Technol.* **2005**, *59*, 138–153.
8. Nisolle, M.; Casanas-Roux, F.; Qu, J.; Motta, P.; Donnez, J. *Fertil. Steril.* **2000**, *74*, 122–129.
9. Kasai, M.; Mukaida, T. *Reprod. Biomed. Online* **2004**, *9*, 164–170.
10. Kerr, W. L.; Kauten, R. J.; McCarthy, M. J.; Reid, D. S. *Lebensm. Wiss. Technol.* **1998**, *31*, 215–220.
11. Harz, H. P.; Weisser, H.; Liebenspacher, F. *DKV-Tagungsber* **1989**, *16*, 741–752.
12. Lucas, T.; Mariette, F.; Dominiawsyk, S.; Le Ray, D. *Food Chem.* **2004**, *84*, 77–89.
13. McCain, D.; Markley, J. L. *Carbohydr. Res.* **1986**, *152*, 73–80.
14. Roos, Y. *Carbohydr. Res.* **1993**, *238*, 39–48.
15. Johari, G. P.; Hallbrucker, A.; Mayer, E. *Nature* **1987**, *330*, 552–553.
16. Blond, G.; Simatos, D.; Catté, M.; Dussap, C. G.; Gros, J. B. *Carbohydr. Res.* **1997**, *298*, 139–145.
17. Terman, F. E. *Radio Engineering's Handbook*; McGraw-Hill: New York, 1943.
18. Mariette, F.; Lucas, T. *J. Agric. Food Chem.* **2005**, *53*, 1317–1327.
19. Searles, J. A.; Carpenter, J. F.; Randolph, T. A. *J. Pharm. Sci.* **2001**, *90*, 860–871.
20. Franks, F. *Water: A Comprehensive Treatise*; Plenum Press: New York, 1982.
21. Hagiwara, T.; Hartel, R. W. *J. Dairy Sci.* **1996**, *79*, 735–744.
22. Sutton, R. L.; Cooke, D.; Russel, A. *J. Food Sci.* **1997**, *61*, 746–748.
23. Chouvenc, P. Optimisation du procédé de lyophilisation d'un complexe lipoprotéique. [Thesis]. Villeurbanne, France: Université Claude Bernard Lyon 1, Thesis, 1999.
24. Hindmarsh, J. P.; Buckley, C.; Russell, A. B.; Chen, X. D.; Gladden, L. F.; Wilson, D. I.; Johns, M. L. *Chem. Eng. Sci.* **2004**, *59*, 2113–2122.